A skeletal mechanism for prediction of ignition delay times and laminar premixed flame velocities of hydrogen-methane mixtures under gas turbine conditions

Yuanjie Jiang[a,*], Gonzalo del Alamo[b], Andrea Gruber[b], Mirko R. Bothien[c], Kalyanasundaram Seshadri[a], Forman A. Williams[a]

[a] *University of California, San Diego, La Jolla, CA, USA*
[b] *SINTEF Energy Research, Trondheim, Norway*
[c] *Ansaldo Energia Switzerland, Baden, Switzerland*

Abstract

The aim of this study is to eliminate unimportant steps from a detailed chemical-kinetic mechanism in order to identify a skeletal kinetic mechanism that can predict with sufficient accuracy ignition delay times and laminar premixed-flame velocities for H_2-CH_4 mixtures under conditions of practical interest in gas-turbine applications, which pertain to high pressure, high reactant temperature, and primarily lean-to-stoichiometric mixture compositions (although somewhat rich conditions also are considered for completeness). The accuracy of selected detailed chemical-kinetic mechanisms that are suited to represent combustion of hydrogen-methane mixtures in air was evaluated through comparison of computed and measured ignition delay times and laminar flame velocities, and because of its relative simplicity and sufficient accuracy, the San Diego mechanism was selected for the needed chemical-kinetic reduction. Under the pressure and temperature conditions of the mixture composition addressed, thirty nine reversible elementary steps involving eighteen species were found to suffice to describe with acceptable accuracy both the ignition delay time and the laminar burning velocities. The skeletal mechanism is given here, along with discussion of its derivation and characteristics, as well as comparison of its predictions with those of the detailed mechanism and, where possible, with experiment.

Keywords: Chemical kinetics, H_2-CH_4 combustion, Flame speed, Ignition delay, Reduced mechanisms

1. Introduction

The development of gas turbines that can be operated with H_2-rich gaseous fuels is considered to be an important step in the implementation of global efforts to reduce carbon emissions [1]. Hydrogen combustion in industrial applications has been conventionally implemented in a manner that incurs increased costs caused by nitrogen dilution or steam injection. These measures are taken to mitigate undesirable effects of the high reactivity of the fuel which creates problems with flame stability and emissions [2, 3, 4]. However, conventional mitigation measures are typically impractical or too expensive to implement when large quantities of pressurized nitrogen or steam are not readily available. Therefore, additional technology development is needed for gas-turbine combustion systems that achieve stable (no thermo-acoustic oscillations), clean (low NO_x), and efficient (dilution-free) combustion of fuels with high hydrogen content [5]. Ultimately, this is a key prerequisite to the viable implementation of power generation solutions in pre-combustion Carbon Capture and Storage (CCS) schemes and in large-scale energy storage based on the use of hydrogen as an energy carrier.

*Corresponding author: Yuanjie Jiang
Email address: yuj056@eng.ucsd.edu (Yuanjie Jiang)

This is the accepted version of an article published in International journal of hydrogen energy
DOI: 10.1016/j.ijhydene.2019.05.068

Recently, considerable progress in this direction was made utilizing Ansaldo Energia's sequential-combustion system with high-hydrogen content fuels [6, 7]. The sequential combustion system, implementing a longitudinal arrangement of two combustion stages separated by a dilution zone [8], enabled combustion of 50-70% (by volume) of H_2 in CH_4, incurring only minor efficiency de-rating and ensuring low-NO_x emissions without the addition of diluents. In this two-stage combustion system, commercially implemented in the GT36 H-class gas turbine, the first stage is based on a propagation-stabilized flame while the second stage consists of a reheat flame, stabilized mainly by auto-ignition [8]. Other manufacturers pursue similar strategies [9, 10] although implementing a somewhat different split of the thermal power between stages. Furthermore, in the process of adapting the gas turbine combustion system to operate on fuels with increasing H_2 content, the fact that the combustion system must be able to handle secondary or back-up fuels, such as natural gas, must be taken into account. This highlights the importance of flexible combustion systems, able to burn variable H_2 contents, ranging from 100% CH_4 to 100% H_2. Accordingly, in the transition between operation with natural gas and hydrogen, the combustion system will have to burn a range of mixtures of these fuels (co-firing) [11, 6, 7]. An additional advantage of multi-stage combustion systems is that these seem to offer the most promising solution for modern power plants that require higher turn-down ratios, part-load efficiency, and fuel flexibility, while still ensuring low pollutant emissions.

In such staged systems, the pressure typically varies between 10 and 30 atm, while the combustor-inlet temperature of the reactant mixture spans a wide range, starting as low as 600 K in the first (premix) combustor and reaching 1400 K in the second (reheat) combustor. The flame temperatures reached in the combustion chamber of the gas turbine depend on the required power output and ranges from 1500 K at part-load conditions to values exceeding 1900 K at full-load conditions. Accordingly, for chemical-reaction kinetic models to be useful in this context, they must provide accurate results throughout these ranges of fuel composition, temperature, and pressure. Also, in the design and optimization of gas-turbine combustors engineers often employ large-scale Large Eddy Simulations (LES) of realistic geometrical models [12, 13, 14]. Beyond that, in recent years, enabled by the wider availability of High Performance Computing (HPC) platforms, Direct Numerical Simulation (DNS) of relevant simplified unit problems [15, 16, 17, 18, 19, 20] has emerged as an additional applied research tool that, complementing LES calculations, is largely unaffected by modelling assumptions. In order to ensure that these numerical-simulation tools yield accurate solutions of the target turbulent-reactive-flow problems, the turbulence model, the turbulence-chemistry interaction model, and the chemical-kinetic mechanism must be validated over the entire range of operating conditions. Unfortunately, for very large grid-node counts, comprehensive chemical-kinetic mechanisms are not computationally affordable [21]. It is therefore important to perform a reduction of the detailed chemistry to produce a simplified kinetic scheme that can still predict the combustion phenomena of interest (typically, ignition-delay times and laminar premixed-flame velocities), with sufficient accuracy at an affordable computational cost. The derivation of simplified kinetic schemes from detailed mechanisms [22] involves the identification of a smaller number of elementary reactions that contribute appreciably to the exothermicity and to the consumption or production of species, so-called skeletal mechanisms, which can be further reduced based on quasi-steady-state approximation of intermediate species if desired.

The main objective of the present work is to derive a simplified kinetic scheme that can be used directly in large-scale numerical simulations (LES and DNS for HPC) of the combustion process that characterizes gas turbines operating with hydrogen and methane mixtures. The approach is to produce a skeletal mechanism, involving a small number of species, that can predict, with sufficient accuracy, ignition delay times and laminar premixed-flame velocities for H_2-CH_4 mixtures under the conditions of interest mentioned above. In this paper, on the basis of a thorough evaluation of the accuracy of the relevant detailed kinetic mechanisms currently available for predicting results of experimental measurements of these quantities, a convenient mechanism is selected and used to perform a sensitivity analysis that serves to identify a set of elementary reactions that involves as few species as possible and that is able to predict, with satisfactory accuracy, ignition delay times and laminar premixed-flame velocities over the entire range of relevant conditions.

This is the accepted version of an article published in International journal of hydrogen energy
DOI: 10.1016/j.ijhydene.2019.05.068

2. Experimental data available

A number of experimental investigations are available in the literature addressing the combustion characteristics of hydrogen and methane mixtures. Concerning autoignition, Herzler and Naumann [23] and Zhang et al. [24] investigated experimentally the ignition delay time in shock-tube experiments using a reference methane-containing gas (92% CH_4, 8% C_2H_6) diluted with Ar, with hydrogen concentration in the fuel mixture of 0%, 40%, 80% and 100% H_2 at pressures, temperatures and equivalence ratio in the range of 0.1 - 2 MPa, 900-2000 K and 0.5-1.0, respectively. These experiments showed a $\sim p^{-0.5}$ dependence of the ignition delay time on pressure p for H_2 blending up to 40%, typical of hydrocarbon systems, and the activation energy decreased as the H_2 concentration was increased, as would be expected. For fuel mixtures containing 80% H_2 and 100% H_2, the ignition delay time exhibited a pressure dependence typical of hydrogen ignition, i.e., a decreasing ignition delay time up to a moderate pressure, then an increase with increasing pressure at higher pressure in the temperature range of interest. Petersen et al. [25], Huang et al. [26] and Chaumeix et al. [27] also used shock-tube experiments to investigate the effect of hydrogen addition up to 40% in methane with lean-to-stoichiometric conditions at pressures of about 20 atm and 40 atm. Fotache et al. [28] investigated ignition delay up to 8 atm with hydrogen fractions up to 60% by volume in a counterflow ignition facility, while Gersen et al. [29] used a rapid-compression machine to investigate ignition delay at even higher pressures (up to 70 atm).

Concerning the experimental investigation of laminar premixed flames, while a considerable amount of data are available for methane-air systems, only one such study [30] reached pressures as high as 10 atm, the lower limit of present interest. Hu et al. [31, 32] studied the laminar burning velocity and onset of cellular instabilities of CH_4-H_2-air flames at pressures up to 7.5 atm, H_2 content from 0 - 100 % and preheat temperatures from 303 - 443 K, while Burke et al. [33] investigated the mass burning rate of H_2-air flames at even higher pressure, up to 25 atm, with high H_2 content 90% and 100% at lean conditions. Halter et al. [34] investigated a wider range of equivalence ratios, but with hydrogen addition only up to 20% and pressure up to 5 atm. Shy et al. [35] studied hydrogen-methane *turbulent* flames up to 5 atm. In general, an increasing concentration of hydrogen in methane leads to faster combustion chemistry, a higher laminar flame speed [36], a thinner flame [34], and a shorter ignition delay time [37].

3. Evaluation of the detailed chemistry

Since the combustion chemistry of both hydrogen and methane are sub-mechanisms of all detailed kinetic schemes for hydrocarbon oxidation, there are numerous sources for detailed hydrogen and methane kinetics. Table 1 lists the detailed mechanisms considered here for making a selection, with their respective number of species and reactions. The San Diego mechanism [38] is intended to be as short as possible, which favors its implementation in CFD simulations. The Princeton mechanism is mainly developed for CO, CH_2O and CH_3OH combustion [39, 40], where the H_2-O_2 subset is the well-known Li-mechanism [41], but the mechanism has also been tested against CH_4 mixtures [33]. The GRI mechanisms [42] are still the most widely used mechanisms for hydrocarbon chemistry. Previous studies [43] have shown that the newest GRI-Mech 3.0 performs sub-optimally for mixtures with high H_2 content; therefore its precursor GRI-Mech 2.11 [44] also was considered in the present work. The mechanisms of [45] with the H_2-O_2 subset of [46] has been shown to perform well for ignition delay of methane-hydrogen mixtures [25, 24], while the USC-II mechanism [47] with the H_2-O_2 subset of [48] has shown reasonable agreement with relevant laminar flame speed measurements [33]. The recently developed HyChem mechanism [49] uses the USC-II mechanism as starting point and performs well in the prediction of ignition delay time for CH_4-H_2 mixtures, but it is less accurate in predicting laminar flame velocities. The mechanism of Konnov [50], which is a well-known hydrogen and hydrocarbon mechanism, was not considered because of its very large size and because of some difficulties encountered in achieving convergence in the calculation of laminar flame velocities. Other large mechanisms, such as the Milano mechanism that was used whenever possible as the starting large mechanism in development of the (smaller) San Diego mechanism, were not included for similar reasons.

The available data from the previously cited literature that were employed for evaluating the overall performance of each of the aforementioned detailed kinetic mechanism is summarized in Table 2 for ignition

This is the accepted version of an article published in International journal of hydrogen energy
DOI: 10.1016/j.ijhydene.2019.05.068

delays and in Table 3 for laminar burning velocities. The Princeton mechanism yields excellent agreement with experimental data in laminar burning velocities; however, it overestimates the ignition delay time by approximate a factor of 2. The Petersen mechanism predicts the ignition delay time fairly accurate, especially around 40 atm. In addition, it obtains accurate flame-speed predictions, except at fuel-rich conditions and high H_2 content (larger than 60%). The GRI 3.0 mechanism significantly underestimates the ignition delay time, underestimates the laminar burning velocity at high H_2 content, and obtains marginal accuracy in laminar burning velocities at other conditions. Compared to GRI 3.0, the GRI 2.11 mechanism exhibits better performance in the prediction of ignition delay time and in the prediction of the laminar burning velocity at low H_2 content. The differences in flame-speed predictions between GRI 2.11 and the San Diego mechanism, the former giving higher velocities, can be explained by the higher chain-terminating reaction rates $H_2 + O_2(+M) \rightarrow HO_2(+M)$ and $HO_2 + H \rightarrow H_2 + O_2$ for the San Diego mechanism; in addition, the production of H-radicals through the chain reactions $OH + CO \rightarrow H + CO_2$ and $CH_3 + O \rightarrow CH_2O + H$ are somewhat faster for GRI 2.11 than for the San Diego mechanism. The San Diego mechanism, USC II mechanism, and HyChem yield the best overall agreement with experimental data over the various conditions. Because of the simplicity and suitability for further reduction, the San Diego mechanism was selected as the starting point to derive a skeletal mechanism consisting of a reduced number of species and elementary reactions.

4. The approach in developing the skeletal mechanism

The approach considered in this paper is to derive systematically a simplified skeletal mechanism that can predict with sufficient accuracy ignition delay times and laminar premixed flame velocities for H_2-CH_4 mixtures under pressure, temperature, equivalence ratio, and H_2 mole fraction of the unburnt mixture in the range 10-30 atm, 600-1400 K, 0.5-1.5, and 0-100% respectively.

The methodology used for derivation of the skeletal mechanism is to identify the elementary reactions and intermediate species that contribute appreciably to the net consumption of reactants, formation of products and rate of heat release along the complete oxidation history. Mathematically, the criteria for including a specific elementary reaction in the skeletal mechanism are written as $\sum_j^{N_{p,i}}\{\widehat{\omega}_{p,ij}\}/\widehat{\omega}_{p,i} \geq 1-\kappa_p$, $\sum_j^{N_{c,i}}\{\widehat{\omega}_{c,ij}\}/\widehat{\omega}_{c,i} \geq 1-\kappa_c$, and $\sum_j^{N_q}\{\widehat{q}_j\}/\widehat{q} \geq 1-\kappa_q$, where $\widehat{\omega}_{c,ij}$, $\widehat{\omega}_{p,ij}$, and $\widehat{q}_j$ represent the time-average consumption and production rate of species i and the net rate of heat release by the elementary reaction j, $\widehat{\omega}_{c,i}$, $\widehat{\omega}_{p,i}$, and $\widehat{q}$ are the overall consumption and production rate of species i, and the overall rate of heat release, respectively. The limits $N_{p,i}$, $N_{c,i}$, and N_q indicate the number of contributing reactions in each summation. The time average is defined as the time integral along the complete kinetic history divided by the total kinetic time. For ignition, the kinetic history ends at the ignition delay time, which is defined as the inflection point in the temperature evolution under isobaric conditions. For premixed laminar flames, the kinetic history is based on distance and defined as the region where the temperature is within the range $[T_u(1+\sigma), T_b(1-\sigma)]$, the subscripts identifying unburnt and burnt conditions, where $\sigma = 0.05$. The constants κ_c, κ_p, and κ_q are tolerances for the accuracy of the skeletal mechanism, taken to be 0.1 in this analysis.

5. Characteristics of the skeletal mechanism

Table 4 lists the steps of the detailed mechanism that are included in the skeletal mechanism; all steps are reversible, with reverse rates obtained from equilibrium constants and forward rates. The skeletal mechanism comprises 39 reversible reactions among 18 species.

For the range of conditions considered in this analysis, most of the elementary reactions for H_2 oxidation chemistry need to be retained. Exceptions are the reactions involving recombination of the O atoms and the attack of H_2O, HO_2, and H_2O_2 by O atoms. The chain-branching reactions $H + O_2 \rightarrow OH + O$, $H_2 + O \rightarrow OH + H$, and $H_2 + OH \rightarrow H_2O + H$ in the $H_2 - O_2$ kinetics, dominate the evolution of the H, O, and OH radicals throughout the range of conditions considered here. At high pressure, the three-body recombination reaction $H + O_2(+M) \rightarrow HO_2(+M)$ exerts an important influence to reduce the overall production of H, OH, and O radicals, by competing with the chain-branching reactions, and, of course,

This is the accepted version of an article published in International journal of hydrogen energy
DOI: 10.1016/j.ijhydene.2019.05.068

it also increases the production of HO_2 radicals. The effects of this recombination reaction become more relevant at lean conditions as a result of the lower net rate of H production by chain branching. At these conditions, the kinetics involving HO_2 in the propagation of H, OH, and O radicals then become relevant. Other elementary reactions involving three-body recombination of H, O, and OH do not have an appreciable contribution to the overall evolution of these radicals but have to be retained in the skeletal mechanism since they contribute significantly to the net rate of heat release.

Consumption of CH_4 mainly occurs through attack by H, OH, O, and HO_2 radicals, as well as initiation by O_2, to produce CH_3, which reacts with those same radicals and O_2 to form the intermediates CH_3O, CH_2O, $T-CH_2$, and $S-CH_2$, or recombines by a third body to form ethane. The consumption of CH_4 with HO_2 appears to be important only at low pressure and very lean conditions. The elementary reactions involving the attack on CH_3 by H to form $T-CH_2$ and $S-CH_2$ and self-recombination of CH_3 to form C_2H_5 need to be retained only for predicting ignition and laminar premixed-flame velocities at fuel-rich conditions and low temperatures, since they have only a small contribution at lean conditions and high temperatures. The recombination to form C_2H_6, on the other hand, is more important in that, in addition, it also affects the ignition delay time at low H_2 content, for example. The CH_3O radical appears to be in steady-state, with rapid decomposition to form CH_2O through a chaperon. the resulting formaldehyde CH_2O then decomposes further by reacting with H, OH, HO_2, and O_2 to form HCO. The attack of CH_2O by HO_2 appears to be important only under high-temperature and high-pressure conditions throughout the entire range of composition. The consumption of HCO occurs by decomposition with a chaperon and by reaction with H or O_2 to form carbon monoxide CO, which oxidizes to CO_2 through the water-gas reaction $CO+OH \rightarrow CO_2+H$. At low pressures and temperatures, the production of HCO by the reaction of CO with H_2 needs to be retained to predict with sufficient accuracy the evolution of HCO. In the derived skeletal mechanism, $T-CH_2$, $S-CH_2$, and the two C_2 hydrocarbons behave only as products, not contributing to the overall combustion kinetics.

6. Evaluation of the performance of the skeletal mechanism

6.1. Ignition delay time

Figures 1-4 compare numerical predictions of the ignition delay time as a function of temperature, for the detailed San Diego mechanism and the 39-step skeletal mechanism, with measurements from shock-tube autoignition experiments listed in Table 2. In general, it is accepted that shock-tube experiments can accurately measure ignition delay times above about 1000 K, but experimental difficulties are encountered at lower temperatures. Non-ideal effects in this type of experiment, such as inhomogeneities in the mixture and the interaction of the shock wave and the boundary layer, are typically small [51] above 1000 K, so the available data can be trusted, no shock-tube data being available at lower temperatures. Although rapid-compression machines are often used to study ignition processes at lower temperatures, no such data have been reported for the fuels of interest, so comparisons with experiments cannot be made at temperatures between about 600 K and 1000 K. Different experiments employ different definitions of ignition delay times, and the present computations are conducted under homogeneous, isochoric, adiabatic conditions employing the experimental ignition criteria when possible. For cases in which the mechanism lacks the species used to measure the ignition delay time in the experiment, the delay is then estimated by calculating the inflection point of the temperature-time curve for the mixture. The numerical simulations are performed using the open-source code Cantera with the Python interface [52]. As a test it was determined that essentially the same results are obtained with the ChemKin code [53].

Figures 1a-1c show a comparison with experiments of [23], which used a reference methane-containing gas (92% CH_4, 8% C_2H_6 diluted with Ar) with hydrogen concentration of 0%, 40% and 80% at pressures from 1 to 16 atm, and equivalence ratios of 0.5 and 1.0. The definition of the ignition delay time in these experimental measurements was the time interval between the arrival of the reflected shock wave and the maximum value of [CH*]. Since the San Diego mechanism does not contain CH*, the inflection point of the temperature-increase profile was selected for these comparisons. Another possibility would have been to select the maximum of the OH-radical concentration during the ignition history, but when the ignition delay

This is the accepted version of an article published in International journal of hydrogen energy
DOI: 10.1016/j.ijhydene.2019.05.068

times are above 1.5 ms, a thermal runaway leading to pressure rise occurs appreciably prior to the maximum OH emission signal, so that the temperature inflection defines the ignition delay time more accurately, although for ignition delay times below 1.5 ms, both criteria give essentially the same predictions [23, 24]. Figures 1a-1c illustrate that the logarithm of the ignition delay time varies approximately linearly with the reciprocal of temperature at low H_2 content. For the mixture with the highest H_2 content, a steeper decrease with increasing temperature is predicted by the detailed chemistry over an intermediate temperature range, resulting in an S-shaped profile. The 39-step skeletal mechanism does not reproduce this S-shape, nor do the experimental data. The largest differences between the predictions of the detailed and skeletal mechanisms occur at the highest temperatures. The differences between both mechanisms and the experimental data are less than a factor of 3 in all cases, the largest deviation occurring in the low-temperature region in Fig. 1c. It has been reasoned that the ideal assumption of constant-volume conditions would lead to overestimation of ignition delay time in the low-temperature region [24], as observed here.

Figures 2a-2e compare numerical calculations with more recent experiments [24], which supplement the experiments from [23] by extending to higher temperatures and pressures, up to 2000 K and 2MPa, respectively. In these experiments the ignition criterion was a sudden rise in OH* emissions[24]. Because of the lack of OH* in the San Diego mechanism, OH was used as the ignition-signal species instead in the computation, the sudden rise being defined as the time at which a straight line having the maximum OH slope reaches zero. The dependence of the ignition time on the experimental criterion is not large for these mixtures; for example, in a representative case the computed ignition time based on the temperature inflection was only 7.5% longer than that based on the sudden onset of OH. Figure 2a shows that, for pure methane, both the detailed and skeletal mechanisms are in the close agreement with measurements. With increasing hydrogen content, that agreement is seen to degrade somewhat in Figs. 2b, 2c, and 2d, with the predictions of the skeletal mechanism beginning to depart increasingly from those of the detailed mechanism at the higher temperatures. At the H_2 content of 80%, seen in Fig. 2e, the situation is very much like that for the corresponding mixture in the previous figure, indicating that the two different experimental ignition criteria produce quite similar results. These first two figures, as well as later ignition-delay figures, show that the predictions of the skeletal mechanism approach those of the detailed mechanism as the temperature decreases, and the differences of the two predictions remain very small between 600 K and 1000 K, where experimental data are unavailable.

Figures 3a-3b show comparisons between the numerical predictions and the experimental results of [25] for mixtures of CH_4 and H_2 at fuel-lean ($\phi = 0.5$) conditions in air with hydrogen concentrations up to 40% and for pressures of 21.1 atm and 23.3 atm, while Figs. 4a-4d compare the calculated ignition delay times with the measurements by [26] for methane-hydrogen mixtures in air at stoichiometric conditions and 16 atm and 40 atm with 15% and 35% H_2 addition. The ignition criterion for the first of these experiments was a rapid rise in CH* emissions, while for the second it was based on the measured increase of pressure P with time t, namely, the maximum value of dP/dt. This same pressure-time criterion was imposed computationally for this second experiment, while, for the first, the isochoric assumption was replaced by an isobaric assumption, with the maximum rate of temperature increase defining the ignition time. Introduction of the isobaric approximation has a small effect but lengthens the predicted ignition delay slightly, improving agreement between predictions and experiment in this case. The experiments employing the dP/dt criterion exhibit a noticeably weaker dependence of the ignition time on temperature than other experiments and also a weaker dependence than is predicted, underscoring likely inaccuracies of this experimental criterion. If those inaccuracies are considered to be experimental, then the agreements provided by both mechanisms are quite good, the skeletal predictions actually lying slightly closer to the experiments.

Finally, as a test of the skeletal mechanism against the detailed mechanism independent of experiments, Fig. 5 shows the predicted variation with hydrogen concentration in fuel mixture of the ignition delay time defined by the isochoric temperature inflection. The results in the top two panels, Figs. 5a and 5b, at 1 atm, well below the pressures of interest here, show the reasonable performance of the skeletal mechanism at this often-considered standard pressure. The results in the bottom two panels, Figs. 5c and 5d, at the highest pressure of interest for these applications, indicate that at the lower temperatures in the range of interest the agreement is even better than at 1 atm, while the largest differences, around a factor of 3, are found at the highest temperature of interest, but only over an intermediate range of

This is the accepted version of an article published in International journal of hydrogen energy
DOI: 10.1016/j.ijhydene.2019.05.068

hydrogen content. It is curious that if the product of the oxygen concentration and the ignition time is plotted instead, as is often done because that product is nearly independent of the oxygen concentration for hydrocarbons, then the extent of disagreement at high hydrogen content is lessened, but some differences remain. This appreciable false inhibiting influence of the hydrocarbon on hydrogen chemistry, which sets in rather rapidly with small additions of methane to hydrogen, is mitigated below 1200 K or 20 atm. Its removal unfortunately would require a much larger mechanism, which would prevent it from being employed in many computational investigations. This deficiency may lead to significant underestimates of flashback tendencies at these intermediate percentages of hydrogen content for high pressure or temperature, which is an effect that should be kept in mind when the skeletal mechanism is employed.

6.2. Laminar burning velocity

Figures 6a-6c compare numerical predictions of laminar premixed-flame velocities with available results from the experimental measurements in the pressure range of interest. These experiments all were performed with reactants at room temperature; there are no data that cover both the pressure and temperature ranges of interest. The calculations were performed with Cantera [52] for the freely propagating one-dimensional adiabatic laminar premixed flame. The Soret effect (species transport by temperature gradients) and multicomponent molecular transport properties were included because these phenomena are important for mixtures with high H_2 content. Grid convergence was tested and ensured for the solutions. The first panel (Fig. 6a), pertaining to methane-air flames, shows that, while the detailed mechanism exhibits reasonable agreement with experiment, the skeletal mechanism underestimates burning velocities by about a factor of 2. The computational results shown in that panel for 3 MPa demonstrate further that the same general extent of discrepancy, which may be acceptable for some purposes, persists at higher pressures. This difference between burning velocities predicted by the detailed and skeletal mechanisms extends over a range of conditions at low hydrogen content.

Although most available data are at lower pressures than those of primary interest, one study [33] involved a number of flame-speed measurements from atmospheric to high (25 atm) pressure, with fuel-lean high-H_2-content flames. Helium was used as the inert gas in those experiments, and its volume fraction was adjusted to maintain the flame temperature at 1600 K. The results, seen in the second and third panels of the figure (6b and 6c), show that the detailed and skeletal mechanisms both give an acceptable representation of the measured flame speed, at both 100% and 90% H_2, although the discrepancies seem to increase a little as the pressure increases at 100% H_2 content. The improved agreement seen here for the skeletal mechanism indicates that it performs much better at high hydrogen content.

Results of experiments [32] have been reported over a wider range of H_2 addition along with some preheating of the reactants (to 373 K), at pressures from normal atmospheric pressure to the lower limit of pressures of gas-turbine interest. These experiments, carried out in air at an equivalence ratio of 0.8, are compared with predictions in Figure 7. Although the temperatures and pressures in these experiments are below those of our stated ranges of interest, these comparisons were analyzed because they are closer to those ranges than any other available data. A significant increase in flame speed is observed when going from pure methane, as seen in the first panel (Fig. 7a), to 80% H_2, as seen in the fourth (Fig. 7d), for all pressures. A flame-speed reduction with increasing pressure is also observed for all fuel mixtures. For low H_2 content (0%-20% H2), as seen in the first two panels, the detailed San Diego mechanism slightly overestimates the laminar burning velocity, and the skeletal mechanism underestimates the experiments. When the percentage of H_2 increases, as shown in the last two panels, the detailed mechanism obtains better agreement with experiments, but the skeletal mechanism exhibits degraded performance, exhibiting underestimates, although to a somewhat lesser fractional extent than is found for pure methane.

Figure 8 compares the variation with hydrogen concentration in fuel mixture of laminar premixed flame velocities obtained from numerical calculations. The conditions selected for this figure fall in the center of conditions of practical interest. The extent of agreement seen here, at 20 atm, is the same as was found at the extremes of 10 atm and 30 atm, and therefore results at these other pressures are not shown. The reactant temperature selected, 700 K is the highest temperature at which a laminar burning velocity can reasonably be defined; at higher temperatures than this the mixture is already reacting to so great an extent at the initial temperature that burning velocities become meaningless, and only autoignition histories are

This is the accepted version of an article published in International journal of hydrogen energy
DOI: 10.1016/j.ijhydene.2019.05.068

relevant. The agreements seen in the figure at this temperature are the same as those that were found at lower temperatures, down to 600 K, the lowest temperature of gas-turbine interest,and therefore results for lower temperatures are not shown. This figure further emphasizes the underestimate of burning velocities predicted by the skeletal mechanism. The underestimate is reduced at high hydrogen content and is seen generally to be less than the previously indicated factor of 2 encountered for pure methane. In general, then, considering both ignition delays and burning velocities, when the predictions of the skeletal mechanism differ from those of the the detailed mechanism, the skeletal mechanism is the lesser reactive of the two.

7. Concluding remarks

The detailed San Diego mechanism, involving 268 reversible chemical-kinetic reactions and 57 species, has shown overall satisfactory accuracy in predicting both ignition delay times and laminar premixed-flame velocities for hydrogen-methane mixtures under pressures, temperatures, and equivalence ratios relevant to gas-turbine operation. Furthermore, because of its simplicity and suitability for further reduction, the San Diego mechanism was selected as the starting point (base mechanism) to derive a skeletal mechanism consisting of a reduced number of species and elementary reactions. Based on sensitivity analysis of the elementary reaction rates for production or consumption rates of reactants and intermediate species, a skeletal mechanism involving 39 reversible reactions and 19 species is obtained. This simplified kinetic scheme is able to predict the ignition delay times reasonably well, although times too long by as much as a factor of 3 may be found from the skeletal mechanism at the highest pressures and temperatures of interest for mixtures with intermediate hydrogen content. The mechanism also predicts laminar premixed flame velocities within a factor of 2, compared the to calculations with detailed chemistry, for a wide range of pressures, 10-30 atm, temperatures, 600-1400 K, equivalence ratios, 0.5-1.5, and hydrogen concentrations in the fuel mixture, 0-100% (the other component being methane). Accordingly, the skeletal mechanism significantly decreases the computational time required, compared with the San Diego mechanism, while maintaining satisfactory accuracy for many purposes. Remaining discrepancies between detailed and reduced chemistry in predicting ignition delay times at the high-temperature, high-pressure limit of gas-turbine-relevant conditions and in predicting laminar burning velocities at initial temperatures of 700 K and below deserve further investigation in the future work.

References

[1] H.-Y. Shih, C.-R. Liu, A computational study on the combustion of hydrogen/methane blended fuels for a micro gas turbines, International Journal of Hydrogen Energy 39 (27) (2014) 15103–15115.

[2] P. Chiesa, G. Lozza, L. Mazzocchi, Using hydrogen as gas turbine fuel, ASME Journal of Engineering for Gas Turbines and Power 127 (2005) 73–80.

[3] J. Duan, F. Liu, Laminar combustion characteristics and mechanism of hydrogen/air mixture diluted with n2+ h2o, International Journal of Hydrogen Energy 42 (7) (2017) 4501–4507.

[4] B. Bazooyar, A. Shariati, M. Khosravi-Nikou, S. H. Hashemabadi, Numerical analysis of nitrogen oxides in turbulent lifted h2/n2 cabra jet flame issuing into a vitiated coflow, International Journal of Hydrogen Energy.

[5] H.-W. Funke, N. Beckmann, S. Abanteriba, An overview on dry low nox micromix combustor development for hydrogen-rich gas turbine applications, International Journal of Hydrogen Energy 44 (13) (2019) 6978–6990.

[6] A. Ciani, M. R. Bothien, B. Bunkute, J. P. Wood, G. Früchtel, Superior fuel and operational flexibility of sequential combustion in ansaldo energia gas turbines, in: Proceedings of Global Power and Propulsion Society â Technical Conference 2019, GPPS-TC-2019-0032, 2019.

[7] M. R. Bothien, A. Ciani, J. P. Wood, G. Früechtel, Sequential combustion in gas turbines â the key technology for burning high hydrogen with low emissions, in: ASME paper GT2019-90798 (in press), 2019.

[8] D. A. Pennell, M. R. Bothien, A. Ciani, V. Granet, G. Singla, S. Thorpe, A. Wickstroem, K. Oumejjoud, M. Yaquinto, An introduction fo the Ansaldo GT36 constant pressure sequential combustor, in: Proceedings of the ASME Turbo Expo, ASME paper GT2017-64790, 2017.

[9] D. J. Wiebe, T. A. Fox, Combustor assembly in a gas turbine engine (2013).

[10] H. Karim, J. Natarajan, V. Narra, J. Cai, S. Rao, J. Kegley, J. Citeno, Staged combustion system for improved emissions operability and flexibility for 7HA class heavy duty gas turbine engine, in: Proceedings of the ASME Turbo Expo, ASME paper GT2017-63998, 2017.

[11] T. Wind, F. Güthe, K. Syed, Co-firing of hydrogen and natural gases in lean premixed conventional and reheat burners (alstom gt26), in: ASME Turbo Expo 2014: Turbine Technical Conference and Exposition, American Society of Mechanical Engineers, 2014, pp. V04AT04A053–V04AT04A053.

This is the accepted version of an article published in International journal of hydrogen energy
DOI: 10.1016/j.ijhydene.2019.05.068

[12] F. Biagioli, Stabilization mechanism of turbulent premixed flames in strongly swirled flows, Combustion Theory and Modelling 10 (3) (2006) 389–412.
[13] F. Biagioli, F. Güthe, Effect of pressure and fuel-air unmixedness on no_x emissions from industrial gas turbine burners, Combustion and Flame 151 (2007) 274–288.
[14] L. Ziani, A. Chaker, Ambient pressure effect on non-premixed turbulent combustion of ch4–h2 mixture, International Journal of Hydrogen Energy 41 (27) (2016) 11842–11847.
[15] A. Gruber, R. Sankaran, E. Hawkes, J. Chen, Turbulent flame–wall interaction: a direct numerical simulation study, Journal of Fluid Mechanics 658 (2010) 5–32.
[16] R. Grout, A. Gruber, H. Kolla, P.-T. Bremer, J. Bennett, A. Gyulassy, J. Chen, A direct numerical simulation study of turbulence and flame structure in transverse jets analysed in jet-trajectory based coordinates, Journal of Fluid Mechanics 706 (2012) 351–383.
[17] A. Gruber, J. H. Chen, D. Valiev, C. K. Law, Direct numerical simulation of premixed flame boundary layer flashback in turbulent channel flow, Journal of Fluid Mechanics 709 (2012) 516–542.
[18] N. Babkovskaia, N. Haugen, A. Brandenburg, A high-order public domain code for direct numerical simulations of turbulent combustion, Journal of Computational Physics 230 (1) (2011) 1–12.
[19] A. Konduri, A. Gruber, C. Xu, T. Lu, A. Krisman, M. R. Bothien, J. H. Chen, Direct numerical simulation of flame stabilization assisted by autoignition in a reheat gas turbine combustor.
URL https://doi.org/10.1016/j.proci.2018.06.084
[20] D. Cecere, E. Giacomazzi, N. Arcidiacono, F. Picchia, Direct numerical simulation of high pressure turbulent lean premixed ch4/h2–air slot flames, International Journal of Hydrogen Energy 43 (10) (2018) 5184–5198.
[21] J. Warnatz, U. Maas, R. Dibble, Combustion. physical and chemical fundamentals, modeling and simulation, experiments, pollutant formation. berlin: Springer. 298 p.
[22] F. A. Williams, Combustion theory, (1985), Cummings Publ. Co.
[23] J. Herzler, C. Naumann, Shock-tube study of the ignition of methane/ethane/hydrogen mixtures with hydrogen contents from 0% to 100% at different pressures, Proceedings of the Combustion Institute 32 (1) (2009) 213–220.
[24] Y. Zhang, Z. Huang, L. Wei, J. Zhang, C. K. Law, Experimental and modeling study on ignition delays of lean mixtures of methane, hydrogen, oxygen and argon at elevated pressures, Combustion and Flame 159 (3) (2012) 918–931.
[25] E. L. Petersen, J. M. Hall, S. D. Smith, J. de Vries, A. R. Amadio, M. W. Crofton, Ignition of lean methane-based fuel blends at gas turbine pressures, Journal of Engineering for Gas Turbines and Power 129 (4) (2007) 937–944.
[26] J. Huang, W. Bushe, P. Hill, S. Munshi, Experimental and kinetic study of shock initiated ignition in homogeneous methane-hydrogen-air mixtures at engine-relevant conditions, International Journal of Chemical Kinetics 38 (4) (2006) 221–233.
[27] N. Chaumeix, S. Pichon, F. Lafosse, C.-E. Paillard, Role of chemical kinetics on the detonation properties of hydrogen/natural gas/air mixtures, International Journal of Hydrogen Energy 32 (13) (2007) 2216–2226.
[28] C. Fotache, T. Kreutz, C. Law, Ignition of hydrogen-enriched methane by heated air, Combustion and Flame 110 (4) (1997) 429–440.
[29] S. Gersen, N. Anikin, A. Mokhov, H. Levinsky, Ignition properties of methane/hydrogen mixtures in a rapid compression machine, International Journal of Hydrogen Energy 33 (7) (2008) 1957–1964.
[30] X. J. Gu, M. Z. Haq, M. Lawes, R. Woolley, Laminar burning velocity and markstein lengths of methane–air mixtures, Combustion and Flame 121 (1-2) (2000) 41–58.
[31] E. Hu, Z. Huang, J. He, H. Miao, Experimental and numerical study on laminar burning velocities and flame instabilities of hydrogen-air mixtures at elevated pressures and temperatures, International Journal of Hydrogen Energy 34 (20) (2009) 8741–8755.
[32] E. Hu, Z. Huang, J. He, J. Zheng, H. Miao, Measurements of laminar burning velocities and onset of cellular instabilities of methane-hydrogen-air flames at elevated pressures and temperatures, International Journal of Hydrogen Energy 34 (13) (2009) 5574–5584.
[33] M. P. Burke, F. L. Dryer, Y. Ju, Assessment of kinetic modeling for lean H2/CH4/O2/diluent flames at high pressures, Proceedings of the Combustion Institute 33 (1) (2011) 905–912.
[34] F. Halter, C. Chauveau, N. Djebaili-Chaumeix, I. Gökalp, Characterization of the effects of pressure and hydrogen concentration on laminar burning velocities of methane-hydrogen-air mixtures, Proceedings of the Combustion Institute 30 (1) (2005) 201–208.
[35] S. Shy, Y. Chen, C. Yang, C. Liu, C. Huang, Effects of H2 or CO2 addition, equivalence ratio, and turbulent straining on turbulent burning velocities for lean premixed methane combustion, Combustion and flame 153 (4) (2008) 510–524.
[36] B. Milton, J. Keck, Laminar burning velocities in stoichiometric hydrogen and hydrogen-hydrocarbon gas mixtures, Combustion and Flame 58 (1) (1984) 13–22.
[37] R. Cheng, A. Oppenheim, Autoignition in methane-hydrogen mixtures, Combustion and Flame 58 (2) (1984) 125–139.
[38] F. Williams, San diego mechanism 2010, Reaction Design, San Diego, CA.
[39] J. Li, Z. Zhao, A. Kazakov, M. Chaos, F. L. Dryer, J. J. Scire Jr, A comprehensive kinetic mechanism for CO, CH2O, and CH3OH combustion, International Journal of Chemical Kinetics 39 (3) (2007) 109–136.
[40] H. Zhao, J. Fu, F. M. Haas, Y. Ju, Effect of prompt dissociation of formyl radical on 1, 3, 5-trioxane and ch2o laminar flame speeds with co2 dilution at elevated pressure, Combustion and Flame 183 (2017) 253–260.
[41] J. Li, Z. Zhao, A. Kazakov, F. L. Dryer, An updated comprehensive kinetic model of hydrogen combustion, International Journal of Chemical Kinetics 36 (10) (2004) 566–575.
[42] G. P. Smith, D. M. Golden, M. Frenklach, N. W. Moriarty, B. Eiteneer, M. Goldenberg, C. Bowman, R. Hanson, S. Song, W. Gardiner Jr, et al., Gri-mech 3.0, URL http://www.me.berkeley.edu/gri_mech.

This is the accepted version of an article published in International journal of hydrogen energy
DOI: 10.1016/j.ijhydene.2019.05.068

[43] T. Weydahl, M. Poyyapakkam, M. Seljeskog, N. E. L. Haugen, Assessment of existing H2/O2 chemical reaction mechanisms at reheat gas turbine conditions, International Journal of Hydrogen Energy 36 (18) (2011) 12025–12034.
[44] C. Bowman, R. Hanson, D. Davidson, W. Gardiner Jr, V. Lissianski, G. Smith, D. Golden, M. Frenklach, M. Goldenberg, Gri-mech 2.11 (2006).
[45] J. De Vries, E. Petersen, Autoignition of methane-based fuel blends under gas turbine conditions, Proceedings of the Combustion Institute 31 (2) (2007) 3163–3171.
[46] M. Ó Conaire, H. J. Curran, J. M. Simmie, W. J. Pitz, C. K. Westbrook, A comprehensive modeling study of hydrogen oxidation, International Journal of Chemical Kinetics 36 (11) (2004) 603–622.
[47] H. Wang, X. You, A. V. Joshi, S. G. Davis, A. Laskin, F. Egolfopoulos, C. K. Law, USC Mech Version II - High-Temperature Combustion Reaction Model of H2/CO/C1-C4 Compounds, URL http://ignis.usc.edu/USC_Mech_II.htm.
[48] S. G. Davis, A. V. Joshi, H. Wang, F. Egolfopoulos, An optimized kinetic model of h2/co combustion, Proceedings of the Combustion Institute 30 (1) (2005) 1283–1292.
[49] H. Wang, R. Xu, K. Wang, C. T. Bowman, R. K. Hanson, D. F. Davidson, K. Brezinsky, F. N. Egolfopoulos, A physics-based approach to modeling real-fuel combustion chemistry-i. evidence from experiments, and thermodynamic, chemical kinetic and statistical considerations, Combustion and Flame 193 (2018) 502–519.
[50] A. Konnov, The effect of temperature on the adiabatic laminar burning velocities of CH4-air and H2-air flames, Fuel 89 (9) (2010) 2211–2216.
[51] E. L. Petersen, R. K. Hanson, Nonideal effects behind reflected shock waves in a high-pressure shock tube, Shock Waves 10 (6) (2001) 405–420.
[52] R. Design, Cantera 2.3.0, 2018, URL https://www.cantera.org/.
[53] R. Design, Chemkin-pro 15101, Reaction Design, San Diego, CA.

Tables and Figures

Mechanxism	N_s	N_R	Reference
GRI-Mech 2.11	49	279	[44]
GRI-Mech 3.0	53	325	[42]
San Diego	57	268	[38]
Petersen	48	427	[45]
USC-Mech II	111	784	[47]
HyChem	114	824	[49]
Princeton	92	612	[40]

Table 1: Overview of the chemical kinetic mechanisms and their most recent references considered in the present work. N_s is the total number of species in the mechanism (including Argon/Helium). N_R is the total number of reactions in the mechanism. C is the number of carbon atoms in the largest hydro-carbon molecule included in the mechanism.

Reference	Year	H_2 in CH_4	Pressure	Temperature	ϕ
[23]	2009	0-100%	1,4 and 16 atm	900-1800 K	0.5, 1
[25]	2005	20,40%	21.1, 23.3 atm	1130-1550 K	0.5
[29]	2008	0-100%	15-70 bar	950-1060 K	1
[26]	2006	15,35%	16, 40 bar	1000-1300 K	1
[24]	2012	0-100%	0.5, 1, 2 MPa	1290-2000 K	0.5

Table 2: Experimental measurements of the ignition delay time of hydrogen-methane mixtures in shock tubes at elevated pressure. Temperature is given in terms of unburnt temperature T_u.

This is the accepted version of an article published in International journal of hydrogen energy
DOI: 10.1016/j.ijhydene.2019.05.068

Reference	Year	H_2 in CH_4	Pressure	Temperature	ϕ
[28]	1997	0-60%	0.2-8 atm	T_u=300 K	1
[30]	2000	0%	0.1-1 MPa	T_u=300-400 K	0.8-1.2
[31, 32]	2009	0-80%	1-7.5 bar	T_u=373-443 K	0.8
[33]	2011	90-100%	1-25 atm	T_a=1400-1800 K	0.7
[34]	2005	0-20%	1-7.5 bar	T_u=298 K	0.8, 1, 1.2

Table 3: Available laminar flame speed data for hydrogen-methane mixtures at elevated pressure. Temperature given either in terms of unburnt temperature T_u or flame temperature T_a.

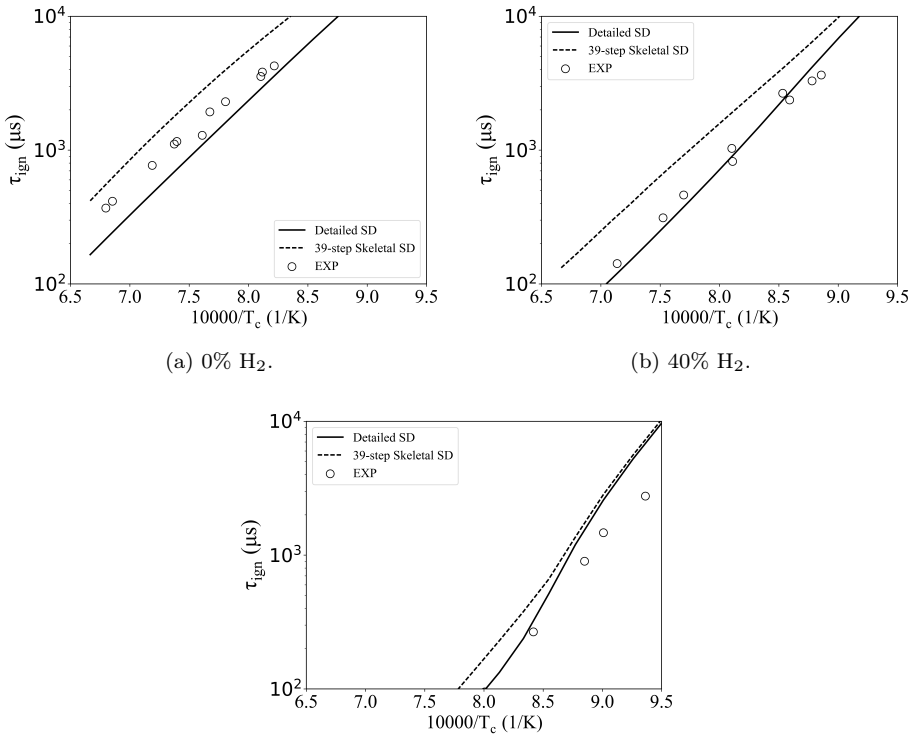

(a) 0% H_2.

(b) 40% H_2.

(c) 80% H_2.

Figure 1: Ignition delay time as a function of initial temperature at $\phi = 0.5$ and 16 bar. The experimental results are from [23] (circles), while the lines represent predicions of the detailed San Diego mechanism (solid lines) and of the 39-step skeletal mechanism (dashed lines).

This is the accepted version of an article published in International journal of hydrogen energy
DOI: 10.1016/j.ijhydene.2019.05.068

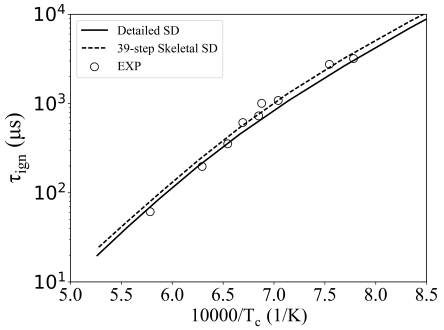

(a) 0% H_2.

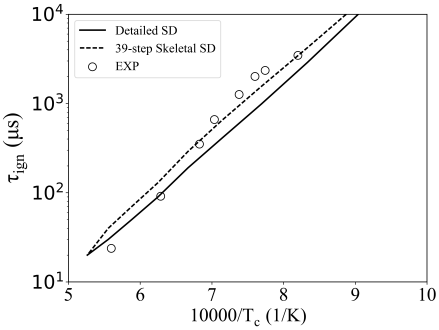

(b) 20% H_2.

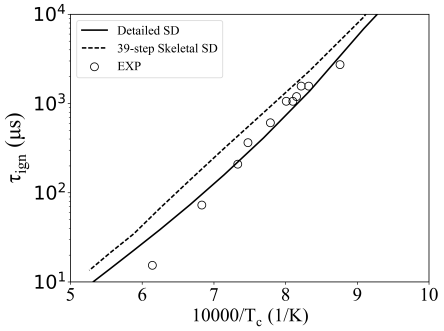

(c) 40% H_2.

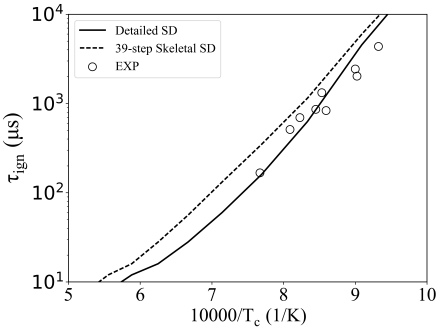

(d) 60% H_2.

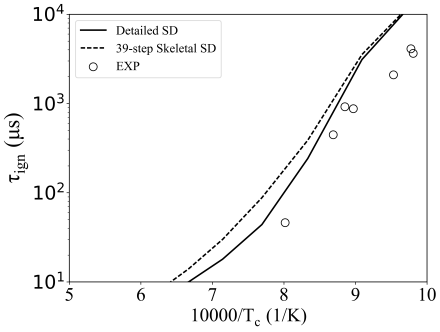

(e) 80% H_2.

Figure 2: Ignition delay time as a function of initial temperature at $\phi = 0.5$ and 2MPa. The experimental results are from [24] (circles),while the lines represent predictions of the detailed San Diego mechanism (solid lines) and of the 39-step skeletal mechanism (dashed lines).

This is the accepted version of an article published in International journal of hydrogen energy
DOI: 10.1016/j.ijhydene.2019.05.068

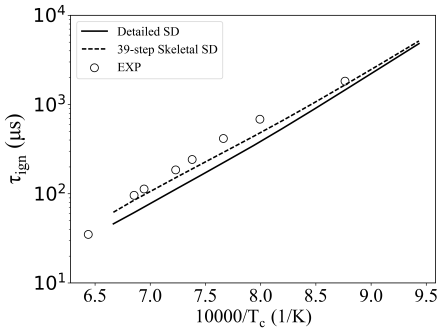

(a) 21.1 atm and 20% H_2.

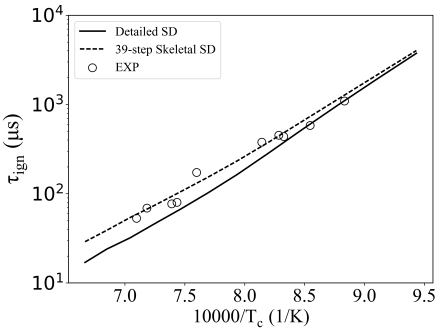

(b) 23.3 atm and 40% H_2.

Figure 3: Ignition delay time as a function of initial temperature at $\phi = 0.5$. The experimental results are from [25](circles), while the lines represent predictions of the detailed San Diego mechanism (solid lines) and of the 39-step skeletal mechanism (dashed lines).

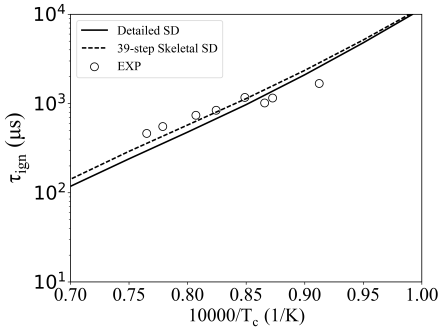

(a) 16 atm and 15% H_2.

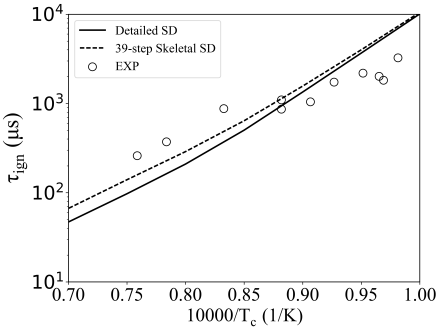

(b) 16 atm and 35% H_2.

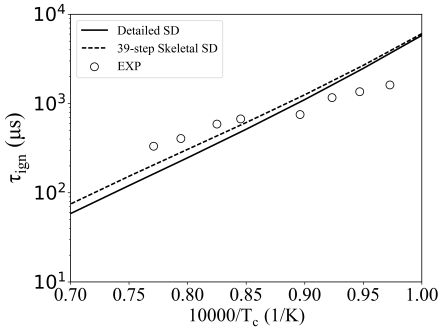

(c) 40 atm and 15% H_2.

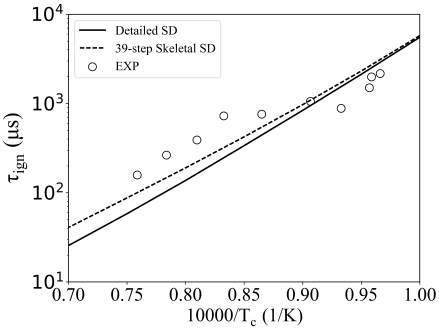

(d) 40 atm and 35% H_2.

Figure 4: Ignition delay time as a function of initial temperature at $\phi = 1.0$. The experimental results are from [26] (circles), while the lines represent predicions of the detailed San Diego mechanism (solid lines) and of the 39-step skeletal mechanism (dashed lines).

This is the accepted version of an article published in International journal of hydrogen energy
DOI: 10.1016/j.ijhydene.2019.05.068

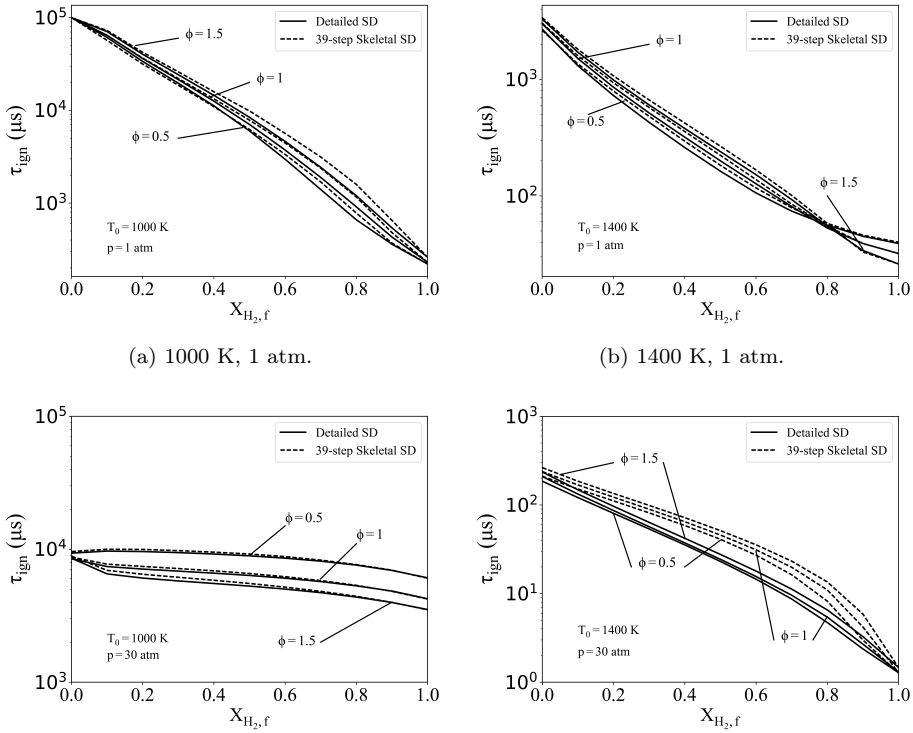

(a) 1000 K, 1 atm.

(b) 1400 K, 1 atm.

(c) 1000 K, 30 atm.

(d) 1400 K, 30 atm.

Figure 5: Variation with the H_2 mole fraction in the fuel of the ignition delay time obtained from numerical calculations using the detailed San Diego mechansim (solid lines) and the 39-steps skeletal mechanism (dashed lines). The pressure, equivalence ratio and temperature of the unburnt mixture are, respectively, 1,30 atm, 0.5-1.5 and 1000 K and 1400 K.

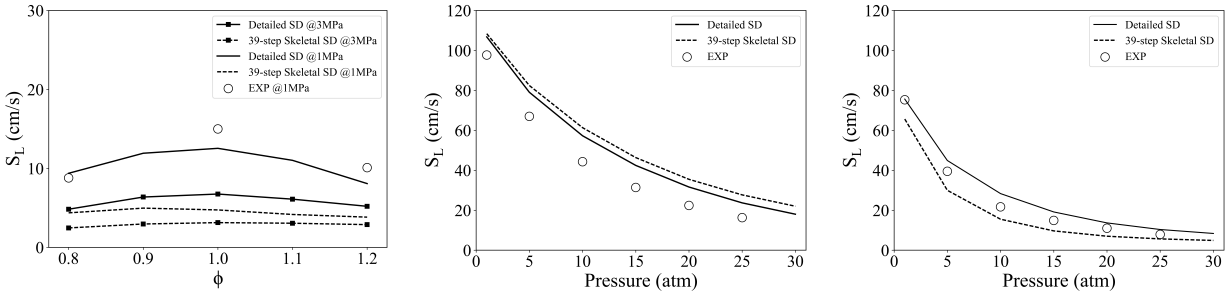

(a) [30], 100% CH_4.

(b) [33], 100% H_2.

(c) [33], 90% H_2.

Figure 6: Laminar burning velocity as a function of equivalence ratio (ϕ) in plot (a) and as a function of pressure in plot (b) and (c) for a range of different conditions.

This is the accepted version of an article published in International journal of hydrogen energy
DOI: 10.1016/j.ijhydene.2019.05.068

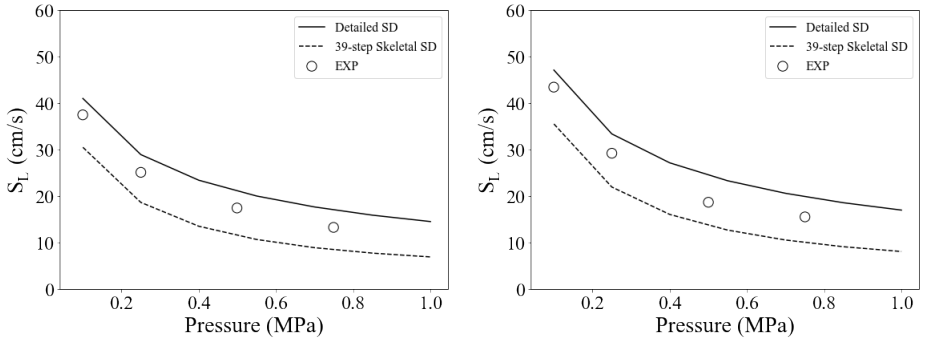

(a) [32], 0% H_2.

(b) [32], 20% H_2.

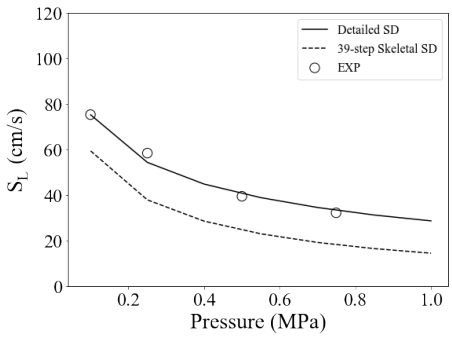

(c) [32], 60% H_2.

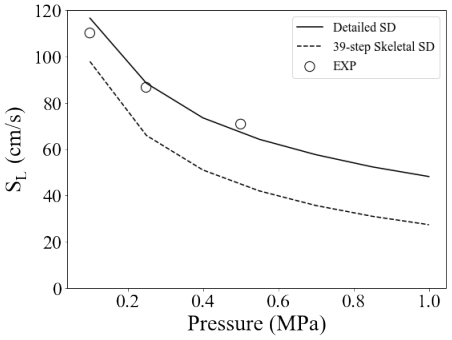

(d) [32], 80% H_2.

Figure 7: Laminar burning velocity as a function of pressure with different H_2 content under 373 K. The experimental results are from [32] (circles), while the lines represent predictions of the detailed San Diego mechanism (solid lines) and of the 39-step skeletal mechanism (dashed lines).

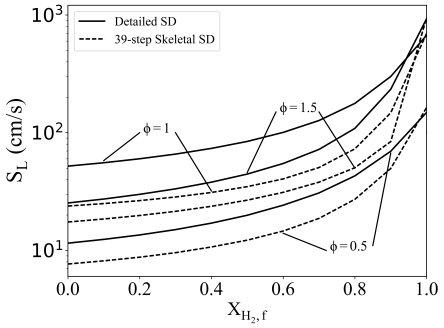

Figure 8: Variation with the H_2 mole fraction in the fuel of the laminar premixed-flame velocity obtained from numerical calculations using the detailed San Diego mechansim (solid lines) and the 39-steps skeletal mechanism (dashed lines) at an unburnt gas temperature of 700 K and a pressure of 20 atm.

This is the accepted version of an article published in International journal of hydrogen energy
DOI: 10.1016/j.ijhydene.2019.05.068

$H + O_2 \rightleftharpoons OH + O$	R1
$H_2 + O \rightleftharpoons OH + H$	R2
$H_2 + OH \rightleftharpoons H_2O + H$	R3
$2H\ (+M) \rightleftharpoons H_2\ (+M)$	R4
$H + OH\ (+M) \rightleftharpoons H_2O\ (+M)$	R5
$H + O + M \rightleftharpoons OH + M$	R6
$H + O_2\ (+M) \rightleftharpoons HO_2\ (+M)$	R7
$HO_2 + H \rightleftharpoons 2OH$	R8
$HO_2 + H \rightleftharpoons H_2 + O_2$	R9
$HO_2 + H \rightleftharpoons H_2O + O$	R10
$HO_2 + OH \rightleftharpoons H_2O + O_2$	R11
$2OH\ (+M) \rightleftharpoons H_2O_2\ (+M)$	R12
$2HO_2 \rightleftharpoons H_2O_2 + O_2$	R13
$H_2O_2 + H \rightleftharpoons H_2 + HO_2$	R14
$H_2O_2 + OH \rightleftharpoons H_2O + HO_2$	R15
$CO + OH \rightleftharpoons CO_2 + H$	R16
$HCO\ (+M) \rightleftharpoons CO + H\ (+M)$	R17
$HCO + H \rightleftharpoons CO + H_2$	R18
$HCO + O_2 \rightleftharpoons CO + HO_2$	R19
$CH_2O + H \rightleftharpoons HCO + H_2$	R20
$CH_2O + OH \rightleftharpoons HCO + H_2O$	R21
$CH_2O + O_2 \rightleftharpoons HCO + HO_2$	R22
$CH_2O + HO_2 \rightleftharpoons HCO + H_2O_2$	R23
$CH_4 + H \rightleftharpoons CH_3 + H_2$	R24
$CH_4 + OH \rightleftharpoons CH_3 + H_2O$	R25
$CH_4 + O \rightleftharpoons CH_3 + OH$	R26
$CH_4 + O_2 \rightleftharpoons CH_3 + HO_2$	R27
$CH_4 + HO_2 \rightleftharpoons CH_3 + H_2O_2$	R28
$CH_3 + H \rightleftharpoons \text{T-}CH_2 + H_2$	R29
$CH_3 + H \rightleftharpoons \text{S-}CH_2 + H_2$	R30
$CH_3 + OH \rightleftharpoons \text{S-}CH_2 + H_2O$	R31
$CH_3 + O \rightleftharpoons CH_2O + H$	R32
$CH_3 + HO_2 \rightleftharpoons CH_3O + OH$	R33
$CH_3 + O_2 \rightleftharpoons CH_2O + OH$	R34
$CH_3 + O_2 \rightleftharpoons CH_3O + O$	R35
$2CH_3 \rightleftharpoons C_2H_5 + H$	R36
$H + CH_3\ (+M) \rightleftharpoons CH_4\ (+M)$	R37
$2CH_3\ (+M) \rightleftharpoons C_2H_6\ (+M)$	R38
$CH_3O\ (+M) \rightleftharpoons CH_2O + H\ (+M)$	R39

Table 4: The 39-step skeletal mechanism derived from the detailed San Diego Mechanism for prediction of ignition delay times and laminar premixed flame velocities.

This is the accepted version of an article published in International journal of hydrogen energy
DOI: 10.1016/j.ijhydene.2019.05.068